Chapter 3

Linear Models from Proper Orthogonal Decomposition

Proper Orthogonal Decomposition (POD), alternatively known as Principal Component Analysis or the Karhunen-Loève decomposition, is a model-reduction technique which generates the optimal linear subspace of dimension D for a given set of higher-dimensional data. That is, if the data are contained within an attractor, the POD process can produce the affine linear space that best approximates the space containing that attractor. In this Chapter, I give a short derivation of the POD algorithm, then show the results from applying it to two different bistable atom-cavity regimes. For each regime, I show the performance of filters based on these POD results.

3.1 Background

The Proper Orthogonal Decomposition (POD) process has been derived in a variety of fields, which has resulted in it having several names. In fluid dynamics, it is known as the Karhunen-Loève decomposition, and has its origins in the work of Lumley [28]. The method itself had its origins in Pearson [29] and again in Hotelling [30].

The derivation which follows is based on those presented by Lall *et al.* [31] and Zhang and Zha [32]. We start with an empirical set of data — an unordered collection of N points $x^{(i)}$ in $\mathbb{R}^m$. In the cases to be examined below, these will be vectorized forms of the density matrix ρ. We would like to build the optimal d-dimensional affine subspace of $\mathbb{R}^m$, which will be isomorphic to $\mathbb{R}^d$. Zhang and Zha take the approach of building the optimal map from the lower dimensional space to the higher, while Lall et al. choose to find the optimal projector from the larger space to the smaller. Here I choose the latter path, because it is more consistent with our goal of projecting the dynamics into the lower-dimensional space.

We would like to find the optimal projection matrix, $Q \in \mathbb{R}^{m\times m}$, from $\mathbb{R}^m$ to a d-dimensional subspace of $\mathbb{R}^m$. We define the optimal Q as that which minimizes the total squared perpendicular

distance of the original set of points from the d-dimensional plane:

$$E(Q) = \sum_{i=1}^{N} \|x^{(i)} - Qx^{(i)}\|^2. \tag{3.1}$$

We wish to find the optimal *affine* subspace, which must go through the mean of the data, so we subtract the mean of all the $x^{(i)}$s, $\bar{x}$, from each point before proceeding. We next construct the correlation matrix

$$R = \sum_{i=1}^{N} (x^{(i)} - \bar{x})(x^{(i)} - \bar{x})^*, \tag{3.2}$$

and calculate its eigenvalues, ordered $\lambda_1 \geq \lambda_2 \geq \cdots \lambda_m$. It is then a standard result that

$$\min_Q E(Q) = \sum_{l=m-d+1}^{m} \lambda_l. \tag{3.3}$$

The magnitude of each eigenvalue measures the relative contribution of the direction corresponding to the paired eigenvector to the data distribution as a whole. By cutting off the space at d dimensions, we measure the error, E, by summing the eigenvalues corresponding to the directions we have chosen to discard.

Turning now to constructing the projector into this optimal subspace, we make use of the orthonormal eigenvectors $\phi_1, \phi_2, \ldots \phi_d$ corresponding to the largest eigenvalues. The approximate $\hat{x}^{(i)}$ to $x^{(i)}$ is given by

$$\hat{x}^{(i)} = \sum_{j=1}^{d} a_{ij}\phi_j + \bar{x} \tag{3.4}$$

where

$$a_{ij} = \left\langle x^{(i)} - \bar{x}, \phi_j \right\rangle. \tag{3.5}$$

Now denote by P the $d \times m$ matrix whose rows are $\phi_1, \phi_2, \ldots \phi_d$. Then the approximant to x is $P^*P(x-\bar{x})+\bar{x}$, and $y = P(x-\bar{x})$ are the new coordinates for x in the new, d-dimensional subspace.

In this derivation, we have assumed an *a priori* known, fixed, d, but in practice one constructs R, and then examines its eigenvalues, choosing d such that the error (3.3) is below whatever threshold one decides.

3.2 Proper Orthogonal Decomposition of quantum trajectories

In attempting to better understand, and approximate, open quantum systems, we might like to find lower-dimensional spaces in which the dynamics are confined, and for this we turn to Proper

Orthogonal Decomposition. Applying the POD process to quantum trajectories requires making a few, nontrivial choices. What space will we define as the larger space of which we seek the optimal subspace? What is the appropriate measure of distance between states, to evaluate the error and optimality of the subspace? A quantum trajectory, in order to be computationally tractable, requires measurement of every output, meaning that states remain pure at all times. We therefore start with wavefunctions, rather than density matrices. However, we know that the experimentalist will almost never have full observation of their system, meaning that she will be working with density matrices.

Density matrices have an amenable algebra, with a clear inner product

$$\langle \rho_1, \rho_2 \rangle = \mathrm{Tr}(\rho_1 \rho_2) \tag{3.6}$$

for use in Eqn. (3.5). In addition, the form that a "direction in density matrix space" will take is clear: a trace-0, Hermitian matrix. For small perturbations of a density matrix by addition or subtract of such a matrix, we know the resulting matrix will almost always remain a valid density matrix — trace 1, positive, and Hermitian. We will see below that large perturbations can result in non-physical density matrices. In contrast, it is not clear how to define a "direction in wave function space."

Of course, the POD algorithm requires its input to be vectors, in order to calculate the correlation matrix R. My process was to create the density matrix corresponding to each wavefunction, $\rho_i = |\psi_i\rangle\langle\psi_i|$, and then to "vectorize" each density matrix. Rather than simply creating a vector which was the end-to-end concatenation of each row or column of ρ_i, I took advantage of the Hermitian structure of the matrix to make a completely real vector by first concatenating the real parts of the rows of the upper-triangular portion of the density matrix, and then concatenating that with the imaginary parts of the upper-triangular portion (aside from the diagonal, which is entirely real). This significantly simplified the computer code necessary to implement the algorithm, and eliminated the chance of error due to confusion of which transpose operations should be complex-conjugate transpositions, and which should be simple transpositions. The * operations in the derivation above are complex conjugate transpositions, but derivations in the literature are not specific on this point, as they assume that everything is simply real. In practice I verified that if one simply unwraps the density matrix, leaving its vector form complex, and treats these as complex-conjugate transpositions, one achieves the same results as I do with the less-mistake-prone real-only method.

I chose a simple Itô-Euler integrator for the propagation of quantum trajectories, as well as for filters. The Quantum Optics Toolbox [10] provides two integrators, an Euler integrator and CVODE. CVODE uses a variable time step, which is incompatible with saving the full homodyne photocurrent record for reuse with the filter. Using the same integration algorithm, with the same time step, is essential for proper functioning of the filter. I used only homodyne detection of the

cavity field and atom because the heterodyne detection portion of the Quantum Optics Toolbox malfunctions: the mean state for a long trajectory is not equal to the steady state solution of the master equation. For the long trajectories (in both phase and absorptive bistability regimes) in this thesis, I chose a small time step, $\Delta t = 5 \times 10^{-6}$, but for shorter trajectories in the phase bistability regime, a time step of as large as 10^{-5} was possible without breeding instability. For absorptive bistability, $\Delta t = 10^{-4}$ was possible for shorter runs. For the test runs for the filters, $\Delta t = 2 \times 10^{-5}$ for absorptive bistability and $\Delta t = 2 \times 10^{-6}$ for phase bistability (which has much faster dynamics than absorptive bistability). The long trajectories took 3 to 4 days to run, with the POD processing taking several hours.

Rather than using the wavevector at every time step for POD, I sampled every N time steps, where N was generally between 100 and 1000 depending on Δt. The time to run the POD algorithm scales linearly with the number of wavevectors used. In order to stay within the memory limitations on the computer (and within the file size limitations of the *matio* C library), I saved the wavevectors in files of roughly 1000. This meant initializing the integrator for many separate, shorter runs, with the initial state of each corresponding to the final state of the previous. The Quantum Optics Toolbox cannot output both operator expectation values and the wavevector from a single run, so when I needed both (such as for the shorter runs used to test the filter), I was forced to run each time slice twice, with the same random seed. The Proper Orthogonal Decomposition algorithm was written in a combination of C and Matlab. I used the *matio* library written by Kevin McHale to read and write Matlab files from C, and took advantage of the BLAS linear algebra library for the matrix multiplication to calculate the correlation matrix R. BLAS can take advantage of the multiple processors on our server, resulting in significant speedup.

This definition of a vector form $\vec{v}$ of ρ is also consistent with the 2-norm for which the optimality of POD is proven:

$$\begin{aligned} \|\rho_1 - \rho_2\|^2 &= \langle \rho_1 - \rho_2, \rho_1 - \rho_2 \rangle = \mathrm{Tr}\left((\rho_1 - \rho_2)^2\right) \\ &= (\vec{v}_1 - \vec{v}_2) \cdot (\vec{v}_1 - \vec{v}_2) = \langle \vec{v}_1 - \vec{v}_2, \vec{v}_1 - \vec{v}_2 \rangle = \|\vec{v}_1 - \vec{v}_2\|^2. \end{aligned} \tag{3.7}$$

As we will see below, however, this distance definition is not necessarily consistent with the accuracy of POD-based filters for particular observables we care most about (such as the expectation values of field quadratures).

The output of the POD algorithm is a set of basis vectors for a density matrix space (a set of trace-0 Hermitian matrices). These are generated from the eigenvectors of the correlation matrix R and each state is associated with an eigenvalue which indicates its relative contribution. We rank the basis vectors according to this eigenvalue, and (as a first cut) discard any state whose eigenvalue falls below 0.1% of the sum of all eigenvalues (the trace of R). For our systems, this commonly leaves

between 10 and 50 eigenstates. Further cuts are always done in the order of increasing eigenvalue, but may be based on the performance of the projected filter or a more subjective sense that the states below a certain eigenvalue look more like noise than states which would significantly contribute to a more accurate approximation.

Proper Orthogonal Decomposition (and various modifications thereof) can produce subspaces which look like they include the relevant parts of the system dynamics. However, we must evaluate them quantitatively. To do this, we project the system dynamics onto several of these subspaces, using the method derived in Section (2.2), and compare the dynamics indicated by the filter with the trajectory dynamics. In this chapter, I use only the normalized dynamical system; the un-normalized system performs slightly less well, and feels slightly less rigorous, due to the necessary renormalization at each time step. The un-normalized projected system also requires re-orthogonalizing the set of states to be used, because the mean state is not orthogonal to the other POD basis states. This in turn means that we lose some of the clarity from the ordering of the states by eigenvalue.

3.3 Phase bistability

The density matrix (and associated Q function) for a phase bistable cavity QED system has a simple structure — roughly, it is the superposition of two compact states with equal amplitude but opposite phase. Q function dynamics consists largely of a compact, roughly Gaussian, peak located at one stable point or the other, or in transition along the path between them. This superficially linear form gives us hope that the linear approximations made in the POD algorithm will not significantly impair performance, and a relatively low-dimensional, high fidelity approximation will be possible. In fact, this hope is largely fulfilled.

Our canonical phase bistable system, used for all of the examples in this thesis, has the following parameter values: $\Theta = 0$, $\Delta = 0$, $\kappa = 4$, $\gamma = 2$, $g_0 = 12$ and $\mathcal{E} = 23.57$. This corresponds to the set of parameters also used in [11]. (Van Handel and Mabuchi use superficially different values, but the ratios determine behavior; in effect I have simply scaled time differently). Expectation values from an excerpt of an example trajectory are shown in Figures 3.3 and 3.4. The trajectory I used to generate the basis states for the subspace onto which we hope to project dynamics was run for 5000 units of time, with a time-step of $\Delta t = 5 \times 10^{-6}$.

The Q functions of the mean (steady state) and the first 11 eigenstates (potential basis vectors) are shown in Figure 3.1. While Q functions for valid quantum states are by definition always positive, the potential basis vectors have Q functions which can swing wildly negative. Recall that these are not quantum states, but rather directions; the Q function is simply an aid to the eye and understanding. A projected state consists of some linear combination of these basis vectors, added to the mean state; the Q functions roughly "add" as well. For example, a state which is composed

by adding the leading eigenstate to the mean would add probability density to one of the two states, while removing it from the other; in effect this first basis direction alone can capture the switching behavior (as we will see in the filter performance evaluation below). Notice that this switching behavior will generally result in rather large components in the direction of this leading eigenstate, threatening the "small perturbation" limit in the linearizing POD process. I get away with this stretching of the POD approximations, I believe, only because the phase bistable system is so simple and symmetric; if the two states were asymmetric I would be forced to undertake the additional complicating procedures I discuss below in the context of (asymmetric) absorptive bistability.

The subsequent states capture behavior within the switching region, or dynamics within one state. The transition basis states take a form similar to sinusoidal peaks and valleys between the two stable states, and we may think of them as the basis states for a Fourier decomposition of a single peak traveling between the two states (behavior which the leading eigenstate cannot capture). Eigenstates beyond the 12th become hard to understand, and their eigenvalues are all less than 0.5% of the sum of all eigenvalues. If we keep the first 12 states, we have kept eigenvalues which sum to 97.3% of the total of all eigenvalues. See Figure 3.2 for a plot of the 60 largest eigenvalues in descending order.

3.3.1 Projection filters

In order to evaluate the performance of the POD-produced approximations, I ran a long, high-resolution (small time-step), quantum trajectory, separate from the trajectory on which the POD algorithm was run. The homodyne photocurrent from the phase quadrature measurement, as well as the expectation values of many system operators, were recorded for comparison with the filter. In addition, I kept 5000 sampled wavefunctions in order to evaluate the fidelity of the approximate states using a variety of measures of quantum fidelity.

Figure 3.3 shows the expectation values for the phase quadrature of the cavity field, $\langle y \rangle$, from a short excerpt of this trajectory, with the quantum trajectory in blue. Comparable traces of $\langle y \rangle$ from filters produced by projecting onto a subspace with 1, 4, 8, and 12 basis states are shown in green, red, cyan, and magenta. Examining these in order, we first see that even a single-dimensional subspace captures the switching behavior of the system (and it does it while stretching the definition of a "small" difference from the mean implicit in our linearized system). However, the 1-D subspace does not capture the transition dynamics between the two states — on the second transition in Figure 3.3, it is closer to a square wave than the decaying exponential of the full trajectory. Adding three basis states, which include some information about states between the two stable ones (see Figure 3.1), allow this transition to exhibit some "decay," while with 8 or 12 states the approximate system can follow the exponential more closely.

Looking now at the first transition, the instabilities of the filter system become apparent. A

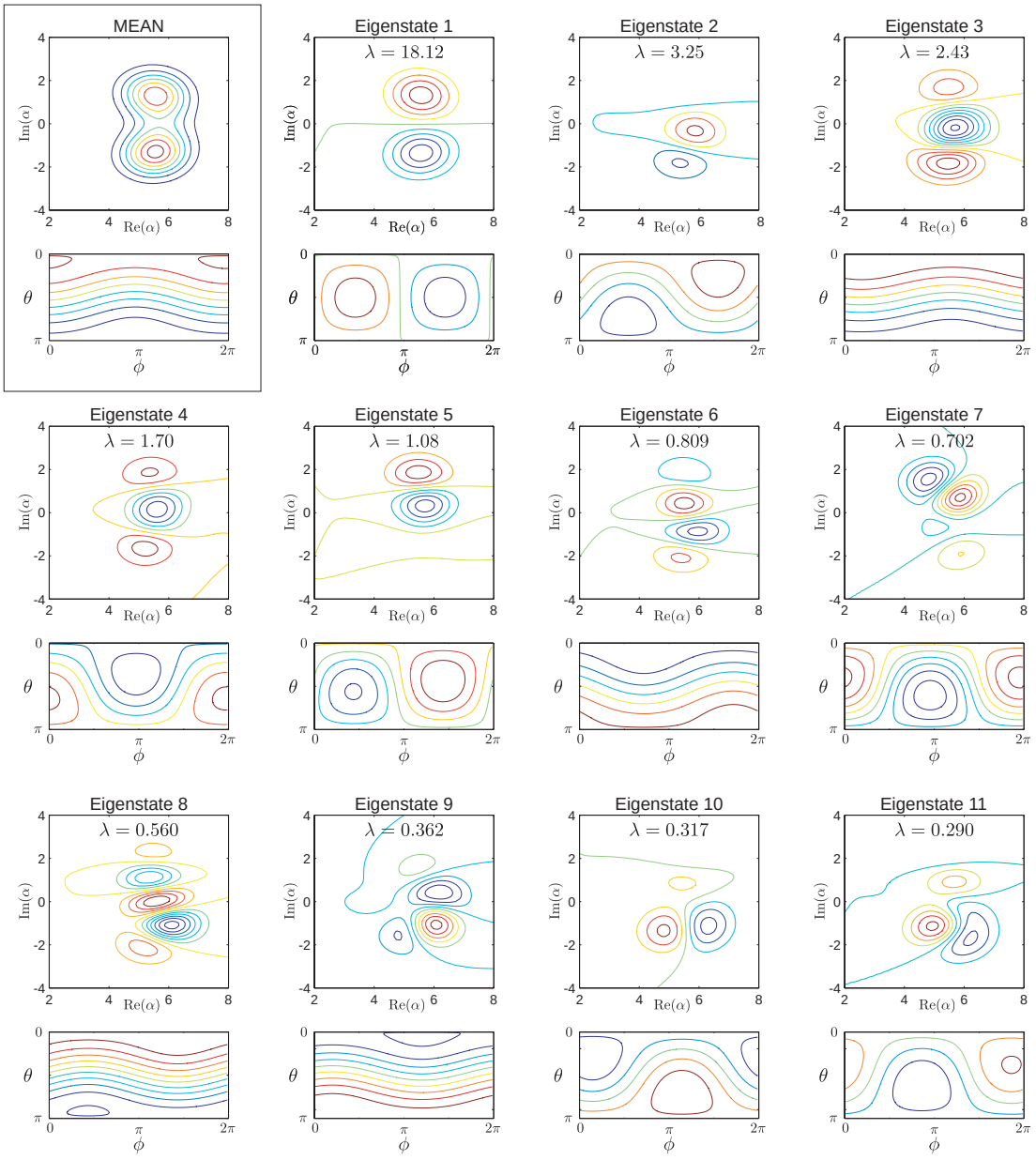

Figure 3.1: Contour plots of Q functions for the mean and the first 11 orthonormal eigenstates from a long phase bistable trajectory. The upper plot for each state is the Q function of the field state after tracing over the atom; the lower plot is the Q function of the atom after tracing over the field (produced using Generalized Coherent States [33]). The eigenvalue corresponding to each eigenstate is included, showing the relative importance of each basis state/direction. The first eigenstate is responsible for most of the switching behavior, whereas the others are largely responsible for motion within each eigenstate (basis states 2, 5, 7, 10 and 11) or the transitions between states (basis states 3, 4, 8, and 9). The atomic Q functions are parametrized on a sphere spanned by $\theta \in [0, \pi]$ and $\phi \in [0, 2\pi]$. Eigenstates 3 and 4 have very similar cavity field effects, and roughly orthogonal atomic states.

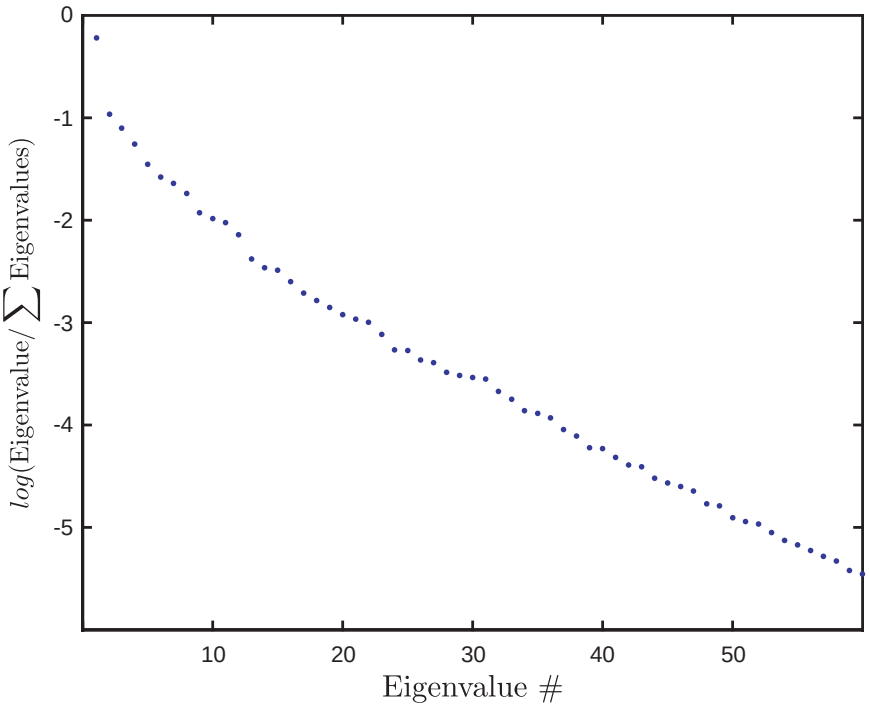

Figure 3.2: Eigenvalues of the correlation matrix R for the canonical phase bistable case, shown as the logarithm of the fraction of total eigenvalues, for the 60 eigenstates with largest eigenvalues.

segment of (noisy) photocurrent here apparently contains relatively little accurate information about the state, the state is only very poorly approximated by the limited subspaces in these 12-or-fewer dimensional approximations, or the photocurrent excites the use of basis states which are not helpful for stability. Similar patches of instability occur with some regularity, and are worst with 12 basis states. In these areas, the filtered state is no longer a valid quantum state (with a positive semi-definite density matrix). Not surprisingly, the fidelity measured between the wavefunction from the quantum trajectory and the projected filter is quite poor in these areas.

I used two fidelity measures to evaluate the performance of this filter: Probability of Error and the Bhattacharyya Coefficient. See Fuchs and van de Graaf [34] for a derivation of these two coefficients, as well as the Kolmogorov Distance (which is intimately related the Probability of Error and doesn't contain any more information). The Probability of Error is defined as

$$PE(\rho_0, \rho_1) = \frac{1}{2} - \frac{1}{4} \sum_{j=1}^{N} |\lambda_j|, \tag{3.8}$$

where λ_j are the eigenvalues of $(\rho_0 - \rho_1)$. This value should vary between 0 (two states are perfectly distinguishable) and 1/2 (perfectly indistinguishable) as long as ρ_0 and ρ_1 are valid density matrices.

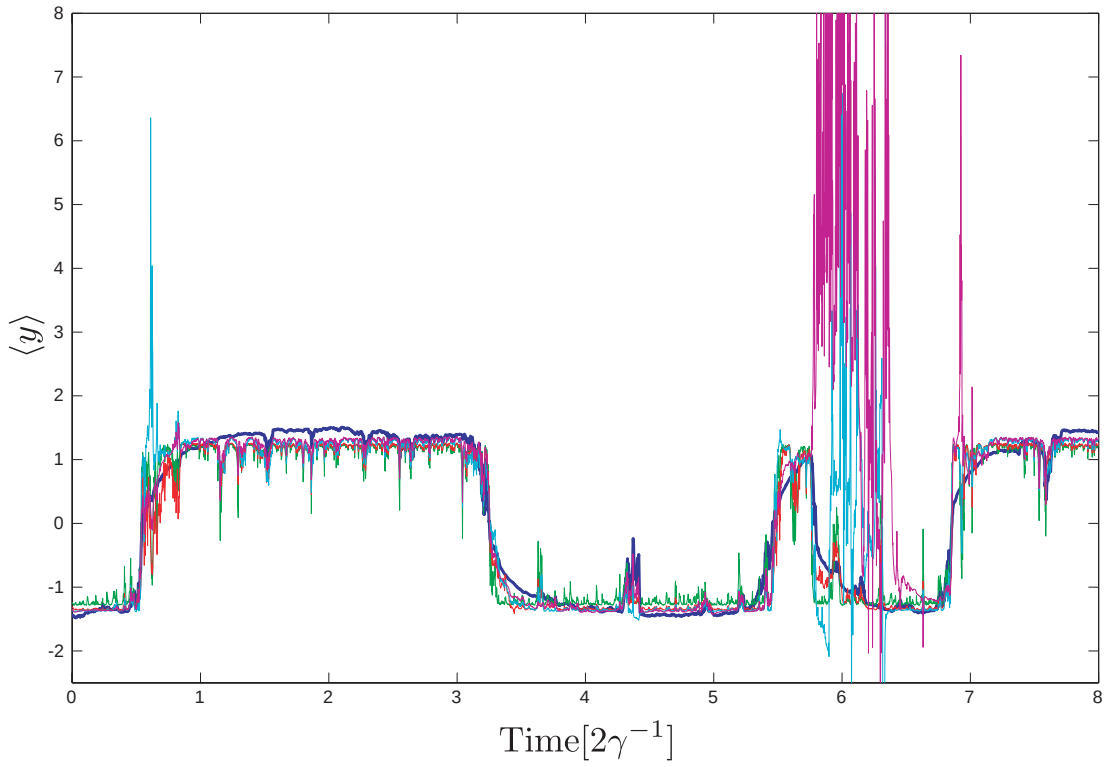

Figure 3.3: A short excerpt from a single phase-bistable quantum trajectory, showing the expectation value of the phase quadrature of the cavity field, $\langle y \rangle$, and the trajectories of three filters using the same homodyne detection photocurrent. The trajectory is in blue, and the projected filters using 1, 4, 8, and 12 basis states are shown in green, red, cyan, and magenta, respectively. The filters with 8 and 12 basis states are somewhat less stable (witness the first and fourth transitions here), but give a closer approximation during the "quiescent" times between transitions, and fit the exponential decay shape of the second transition better than the 1 or 4 basis-state approximations. Projecting onto even a one-dimensional subspace, however, successfully captures the switching behavior of the system.

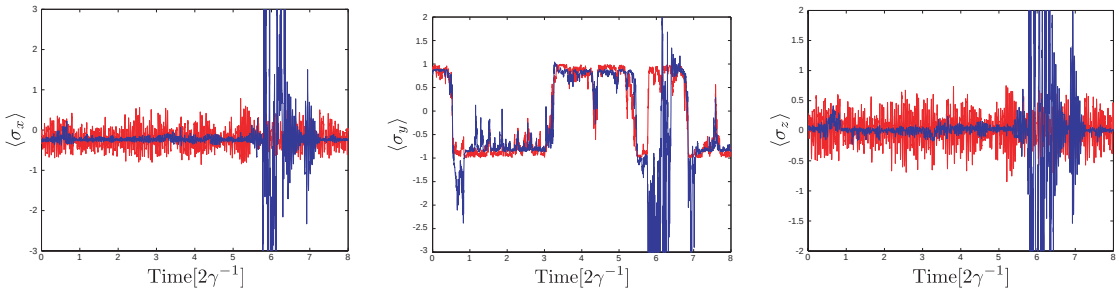

Figure 3.4: Trajectories of the three simple atomic Hermitian observables for the same time span as Figure 3.3. (a) σ_x, (b) σ_y, and (c) σ_z. For each observable, the red trace is the quantum trajectory; the blue trace is the filter with 12 basis states (the same filter as shown in magenta in Figure 3.3).

The Bhattacharyya Coefficient is defined as

$$B(\rho_0, \rho_1) = \mathrm{Tr}\sqrt{\sqrt{\rho_0}\rho_1\sqrt{\rho_0}}. \tag{3.9}$$

Its value varies between 0 (orthogonal states) and 1 (identical states).

The calculated values of these two fidelity measures over the course of an extended filtering simulation offer some surprises, which indicate both the failures of the filter, and differences between these two measures. The average Probability of Error decreases as we include more states in our basis, from 0.2065 with one basis state, to 0.2059 with 4, 0.1057 with 8 and *-0.0708* with 12. What is happening is that the periods of instability are dominating the average. In these areas, the approximate state is not a valid quantum state, and the value of the "probability" can fall below zero. However, if we examine just the quiescent periods between state transitions and unstable patches, the Probability of Error is almost identical for the four filters.

The Bhattacharyya Coefficient (BC) behaves somewhat differently. In particular, when the filter state becomes unphysical, the BC becomes imaginary, rather than negative (I use only the real part of the BC, as the mean of the imaginary parts is very close to zero). This allows the average value over a filtering run to stay almost constant with the size of the basis state, because the 12-dimensional basis does provide for a slightly higher BC than the 8 in the "normal" periods, which in turn has a higher BC than the 4- and 1-state filters. The unstable zones have a BC of zero, so the increased instability from added basis states results in a falling average. The 1 state BC is 0.4364, 4 state BC is 0.4485, 8 state is 0.4463, and 12 state is 0.4355.

Proper Orthogonal Decomposition appears to work quite well to define a subspace in which the phase bistable dynamics take place. The basis states (in Figure 3.1) capture both stable states, and allow for approximations of both the dynamics within each state and the transitions between. When stable, the projected filter can do a good job of matching the behavior of $\langle y \rangle$ and $\langle \sigma_y \rangle$; other observables fluctuate quickly, while the filter approximates their mean. The occasional instability of the filter, however, raises doubts as to whether POD is a robust solution.

3.4 Absorptive bistability

Absorptive bistability occurs as part of a much more complicated system than phase bistability. In particular, the upper "state" is extended for our set of parameters (very different from the close-to-minimum-uncertainty states in phase bistability). Complicating the performance of the Proper Orthogonal Decomposition algorithm, the system can be significantly asymmetric between the upper and lower states, depending on the driving field strength (phase bistability is structurally exactly symmetric). I have chosen a driving field for the examples in this thesis at which the fraction of time

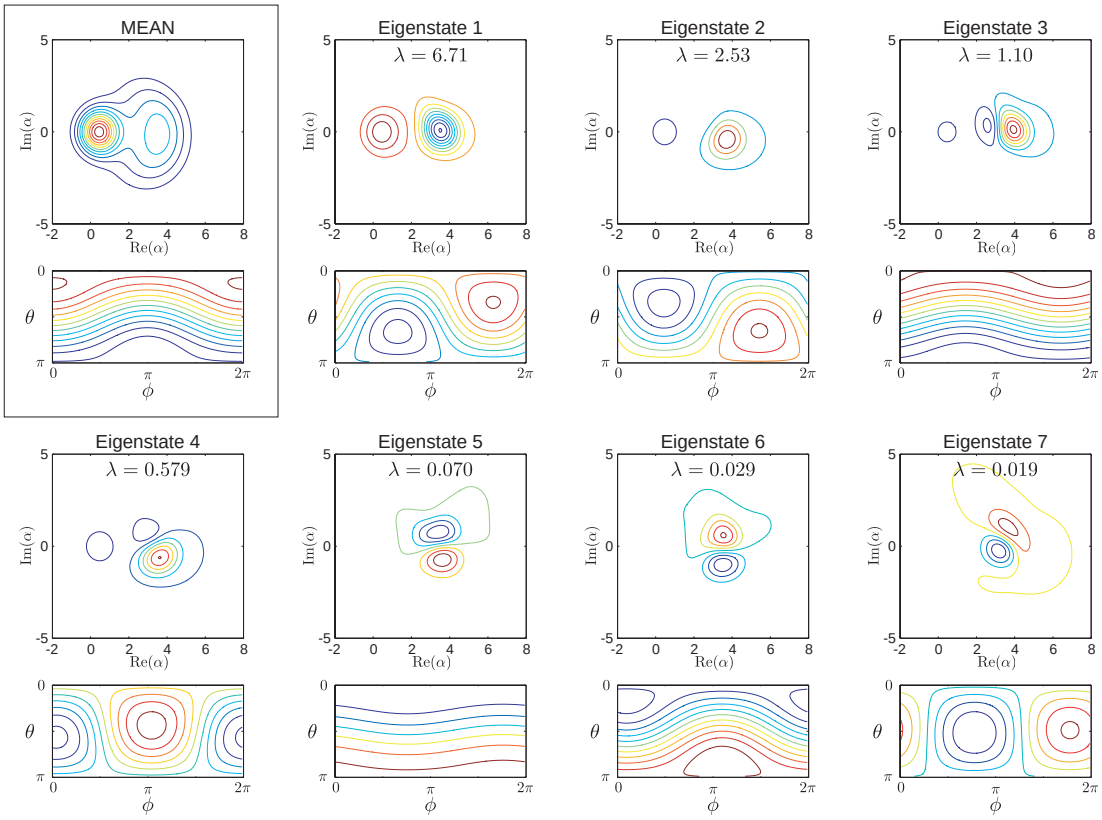

Figure 3.5: The mean and leading 7 eigenstates from the Proper Orthogonal Decomposition algorithm applied to a long absorptive bistable trajectory. The first eigenstate allows the filter to remove almost all traces of the lower state, while the remaining eigenstates finish that cancellation and allow for dynamics within the upper state. No combination of these states, however, allows for the cancellation of the full upper state in order to accurately approximate the lower stable state. The model parameters are $\Theta = 0$, $\Delta = 0$, $\kappa = 0.1$, $\gamma = 2$, $g_0 = \sqrt{2}$, and $\mathcal{E} = 0.56$, and the simulation was run for $t_{final} = 5000$ (with time scaled by $\gamma/2$).

spent in each state is roughly equal; however, this may not be the experimentalist's preferred (or available) parameter value, resulting in lower POD performance unless the algorithm is extended, as I will describe later in this subsection.

The parameters I have chosen to demonstrate the application of POD to an absorptively bistable system are: $\Theta = 0$, $\Delta = 0$, $\kappa = 0.1$, $\gamma = 2$, $g_0 = \sqrt{2}$, and $\mathcal{E} = 0.56$. (This is clearly a "good cavity" relative to our phase bistable system; we achieve similar cavity field amplitudes for almost 2 orders of magnitude less driving field intensity.) Notice that this driving field strength is above the upper semi-classical (Maxwell-Bloch) bifurcation point ($\mathcal{E} \approx 0.553$); that is, the semi-classical system has only one stable point at this driving field value. These are similar to the parameters chosen by [22], except I have chosen a slightly lower driving field in order to get closer to an even balance between the lower and higher amplitude states.

Simply applying the POD algorithm to a long ($t_{final} = 5000$) trajectory (with homodyne measurement of field amplitude quadrature) results in the set of states shown in 3.5. Note that the

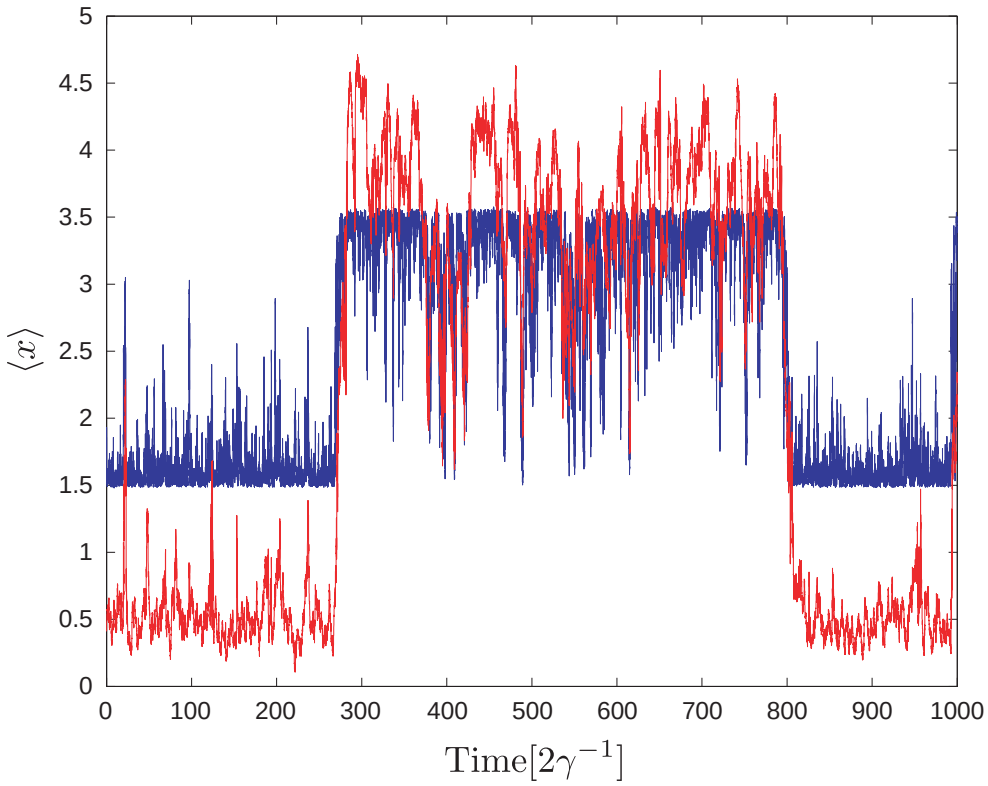

Figure 3.6: Comparison in the absorptive bistability regime of simple POD filter with exact quantum trajectory. The blue trace is the expected value of the amplitude quadrature for a POD filter with a 7-dimensional linear subspace; the red trace is from the quantum trajectory. The eigenvalues corresponding to these leading 7 eigenstates sum to 99.85% of the sum of all eigenvalues; the largest eigenvalue left out is less that 0.08% of the total. Amplitude quadrature homodyne measurement; params.

states beyond the first generally relate to directions in the upper state, and none of these first 8 basis vectors allow for dynamics or fluctuations within the lower state. We know from observing the trajectory that what dynamics there are within the lower state are smaller in amplitude than those within the upper state. The first eigenstate is generally responsible for the switching behavior: subtract this from the mean to move towards the upper state alone, and add it to move toward the lower state alone. Note, however, that the shape of the upper portion of this basis state does not match the shape of the upper portion of the mean, so that adding this state alone will not put us exactly in the lower state. The shapes match much more clearly for the lower state, so if we subtract the correct multiple of this basis state from the mean we can almost exactly cancel the lower state. The second and higher basis states allow for some fluctuations within the upper state.

This asymmetry between the lower and upper states results in significantly impaired performance as a filter. Using 7 eigenstates to make the basis of the subspace into which we project the dynamics, we plot $\langle x \rangle$ from the projected dynamics in Figure 3.6. The eigenvalues corresponding to these leading 7 eigenstates sum to 99.85% of the sum of all eigenvalues; the largest eigenvalue eliminated

is less that 0.08% of the total. The filter tries to match the field amplitude of the lower state, but simply cannot, because the subspace does not include a good approximation to the lower state. The mismatch in shapes results in a minimum achievable $\langle x \rangle$ which is above that of the lower state. The filter does relatively much better with the upper state, although it cannot capture all of the volatility. It is able to track some of the fluctuations down from the upper state, but cannot go higher than a fixed value. It is also unable to track the volatility in $\langle y \rangle$ within the upper state (not shown).

Needless to say, the fidelity of this filter is quite poor. The mean Probability of Error is negative (-0.008), thanks to long periods (in the lower state) in which the filter state is not a valid density matrix (negative eigenvalues, and the Q function not positive everywhere). The Probability of Error measure is positive during the times when the system is in the upper state, averaging around 0.02, with a maximum of 0.155. The mean Bhattacharyya Coefficient is 0.185, with an average of about 0.13 in the lower state, and 0.24 (but wildly varying between 0.012 and 0.6) in the upper state. The resilience of the Bhattacharyya Coefficient to unphysical filter states makes it a somewhat preferred measure.

Some trajectories randomly spend a larger fraction of their time in the lower state than the one I used here, and these trajectories can exhibit the opposite problem as a filter: they capture the lower state and its dynamics well, but badly miss the upper state. In order to address this problem, I tried two different strategies: weighting the sum used to calculate distances in the density matrix space, and dividing the data into three "zones": lower, transition, and upper, and executing POD separately in each zone.

3.4.1 Weighted POD

The observables we tend to care most about in evaluating the accuracy of our model reduction are the 5 observables whose dynamics can be approximated by the Maxwell-Bloch equations: $\langle x \rangle$, $\langle y \rangle$, $\langle \sigma_x \rangle$, $\langle \sigma_y \rangle$, and $\langle \sigma_z \rangle$. In matrix form (to act on density matrices), the nonzero terms for these observables lie on the diagonal or immediate off-diagonal. (For a tensor product system like an two-level-atom and cavity system, let us define the "diagonal" to be the diagonal of each quadrant.) The values of these observables (calculated as $\mathrm{Tr}(\mathcal{O}\rho)$ for each operator $\mathcal{O}$), then, depend only on the diagonal and immediate off-diagonal terms in the density matrix. Proper Orthogonal Decomposition, on the other hand, treats every entry in the density matrix identically. POD produces the optimal subspace provided that we share its definition of distance, which treats the real and imaginary parts of each entry in a completely even-handed fashion. The failure of POD to produce a single subspace which includes both the upper and lower states can be partly attributed to this evenhandedness: dynamics within the upper state win out over including an accurate approximation for the lower state.

To address this, I tested various re-definitions of distance by weighting the terms of the density

matrix. To do this, I defined the distance from the diagonal n_d to be the the absolute value of the difference between i and j labels for each entry in the matrix (modulo half the matrix size to allow for the tensor product structure). I then divided each entry by n_d^X where $X = 0.5$, 1, or 2. This process treats the diagonal differently from the immediate off-diagonal, so I also used a weighting scheme which measured distance from the immediate off-diagonal, so that the weighting would follow the pattern (B) 1, 1, 1/2, 1/3, 1/4, ... instead of (A) 1, 1/2, 1/3, 1/4, ... as we proceed away from the diagonal. None of these six weighting schemes has any appreciable effect on the balance between the upper and lower states, relative to basic POD ($X = 0$). All produce basis states similar to those shown in Figure 3.5, with only dynamics of the upper state represented, and fail as filters because they cannot come close to approximating the lower state.

There is another inequity between the distribution of density matrix entries and the distribution of expectation values: the density of Fock states scales like the square of the amplitude of a coherent state, so that a state further from the vacuum has large entries in many more locations in the density matrix than one close to the vacuum. Imagine two pairs of states, one pair close to the vacuum, and one with $\langle x \rangle \approx 4$. The distance within each pair, when measured in the way we defined for Proper Orthogonal Decomposition, is the same. However, the pair close to the vacuum will have substantially different expectation values, while the higher amplitude pair might be almost indistinguishable by that measure. What skews POD is the reverse of this: small fluctuations in expectation values at high amplitude look like large distances in the POD metric, while small fluctuations near the vacuum are small in this metric. This is compounded by the behavior in the absorptive bistability regime, which has larger fluctuations in the upper state, and the POD process outputs states which focus on the upper state and do a very poor job in the lower.

To counteract this, I tried a weighting scheme which weights the vacuum state highest, and decays away from there. We know *a priori* that the scaling should go like the square root of the Fock state in order for the distance to be independent of the coherent amplitude. Applied to the POD process, this weighting also has no appreciable effect on the fundamental problem: the lower state is not accurately approximated by combinations of the dominant eigenstates. This makes sense because at the same time that this weighting reduces the effective distance between density matrices within the upper state, it also undercounts the remnants of the upper state which are left behind when using the leading eigenstate (see Figure 3.5) to attempt to approximate the lower state. For weighted POD to improve on the unweighted process, we would need a weighting scheme which somehow simultaneously counts and discounts the higher-field-amplitude portions of the density matrix. One possibility, unexplored in this thesis, would be to move the origin for the POD analysis to the space between the lower and upper "states," so that they both have similar amplitude and take up similar "space" within the density matrix. They will still be asymmetric, however, in both shape and the time the system spends in each (especially if the driving field is not selected for balance between

states). Fundamentally, Proper Orthogonal Decomposition with a single mean, and perturbations around that mean, has difficultly handling dynamics around two separated, asymmetric states.

3.4.2 Zoned POD

Proper Orthogonal Decomposition implicitly makes "small perturbation" assumptions, which we violate when we consider a system with multiple stable points, as the leading eigenstates end up with quite large coefficients to push unto into one stable regime or another. In addition, the algorithm's emphasis on the dominant, most common states means that it tells us almost nothing about the transitions between states when there are significant dynamics within states. The phase bistable system considered in Section 3.3 is symmetric enough, and switches often enough, that the switching dynamics and the transition periods are on a more level footing with fluctuations and dynamics within each state. The absorptive bistability regime is not symmetric, and transitions are much more rare. We can improve compliance with assumptions, capture some transition behavior, and re-balance asymmetry by diving the data into *zones* surrounding each stable point, and in between them.

For the driving field strength, cavity damping rate, and other parameters which define our standard absorptive bistability regime, the lower state has a mean cavity field amplitude of about 0.5, and the upper state (while broader) has a mean of about 3.25. The fluctuations around these two states rarely cross into the range of 1.5 to 2.5 unless the system is actually in transition between the two stable regions. Therefore, I cut the data into three sets: "lower" for any point in the trajectory which has $\langle x \rangle < 1.5$, "upper" for points with $\langle x \rangle > 2.5$, and "transition" for points in between. (I include a short segment on either side of the exact transition zone to associate behavior leading to or out of transitions with them, rather than with the lower or upper zones.) Note that the constant measurement and decay of the system helps keep the field states compact. They are almost always roughly Gaussian (with a Q function width similar to the width of a coherent state), so we can use $\langle x \rangle$ as a proxy for the full distribution.

Once we have divided the data into three subsets, we have two options for defining the mean state for the POD algorithm: we could continue to use the overall mean, or find the mean of each zone. In the former case, the leading eigenstate will be the direction from the overall mean to some part of that zone, and subsequent basis states provide a direction within the zone. The latter case creates the transition direction directly, without use of POD, simply by subtracting the zone's mean from the overall mean. All the POD basis states are then directions away from that local mean. I have tried both definitions, but selected the latter because it is most consistent with the small-coefficient assumptions built in to POD and because the means will be independent of small asymmetries which might otherwise throw the leading eigenstate "off balance." This is particularly a concern for the transition zone, where the relatively small number of transitions means that if more transitions take

place with $\langle y \rangle > 0$ than $\langle y \rangle < 0$, the "one mean" algorithm would likely select the leading eigenstate to reflect just the $\langle y \rangle > 0$ transitions, biasing all the subsequent eigenstates as well.

The output of three separate POD processes (one for each zone) is three sets of Hermitian matrices, from which we will build our subspace. (Implementation of the algorithm tends to produce matrices which are almost but not exactly Hermitian, due to numerical errors; I added a simple step which tweaks them to be exactly Hermitian.) There are four matrices with trace 1 (valid density matrices): the overall mean and the mean of each zone. I turn the zone means into trace-0 (direction) matrices by subtracting the overall mean. The remaining matrices are already directions in density matrix space, but they are not all orthonormal. The directions within each zone are orthogonal (although not orthogonal to the newly-created "mean direction" for that zone), but they are not orthogonal between zones. We therefore run the set of all trace-0 direction matrices (including the means) through a simple inner-product based orthonormaliztion process. Because they are all Hermitian, their inner products are all real, and their linear combinations with real coefficients produce new, orthonormal, direction matrices which remain Hermitian. The linear combinations which result from filtering will therefore be valid density matrices as long as they remain positive definite.

Figures 3.7 and 3.8 show the leading states from two different trajectories in the absorptive bistability regime. Figure 3.7 results from a trajectory in which the cavity field was measured in the amplitude quadrature; Figure 3.8 was measured in the phase quadrature. (Note that both show their set of states before they have been orthonormalized.) Because the steady states and behavior of a quantum system do not depend on the measurement, it's not surprising that these two sets of states are quite similar. They do provide an opportunity to examine the some of the kinds of differences which result from different trajectories. For example, the lower zone eigenstates are arranged at different angles, indicating that the noise in the lower state scattered more in one axis than another during the trajectory.

In both cases, the transition zone is biased towards $\langle y \rangle > 0$ behavior in its leading eigenstates. Each of these trajectories include only a dozen or so transitions, meaning that the statistics are quite poor. A much longer trajectory (which would require a more patient researcher and/or a more powerful computer) ought to have more balanced eigenstates in the transition zone. These higher-quality eigenstates might allow us to see whether transitions favor particular paths in phase space. In particular, the semi-classical Maxwell-Bloch equations have an unstable point between the two stable equilibria (see Figure 1.2), and these transition states might reveal whether the quantum system avoids the $\langle y \rangle = 0$, $\langle x \rangle \approx 2$ area, or not. I cannot draw conclusions on this point from the limited trajectories I have been able to analyze.

To test the performance of these POD subspaces, I ran them as a filter on the same homodyne photocurrent as in Figure 3.6 and the surrounding discussion. A disadvantage of the zoned approach

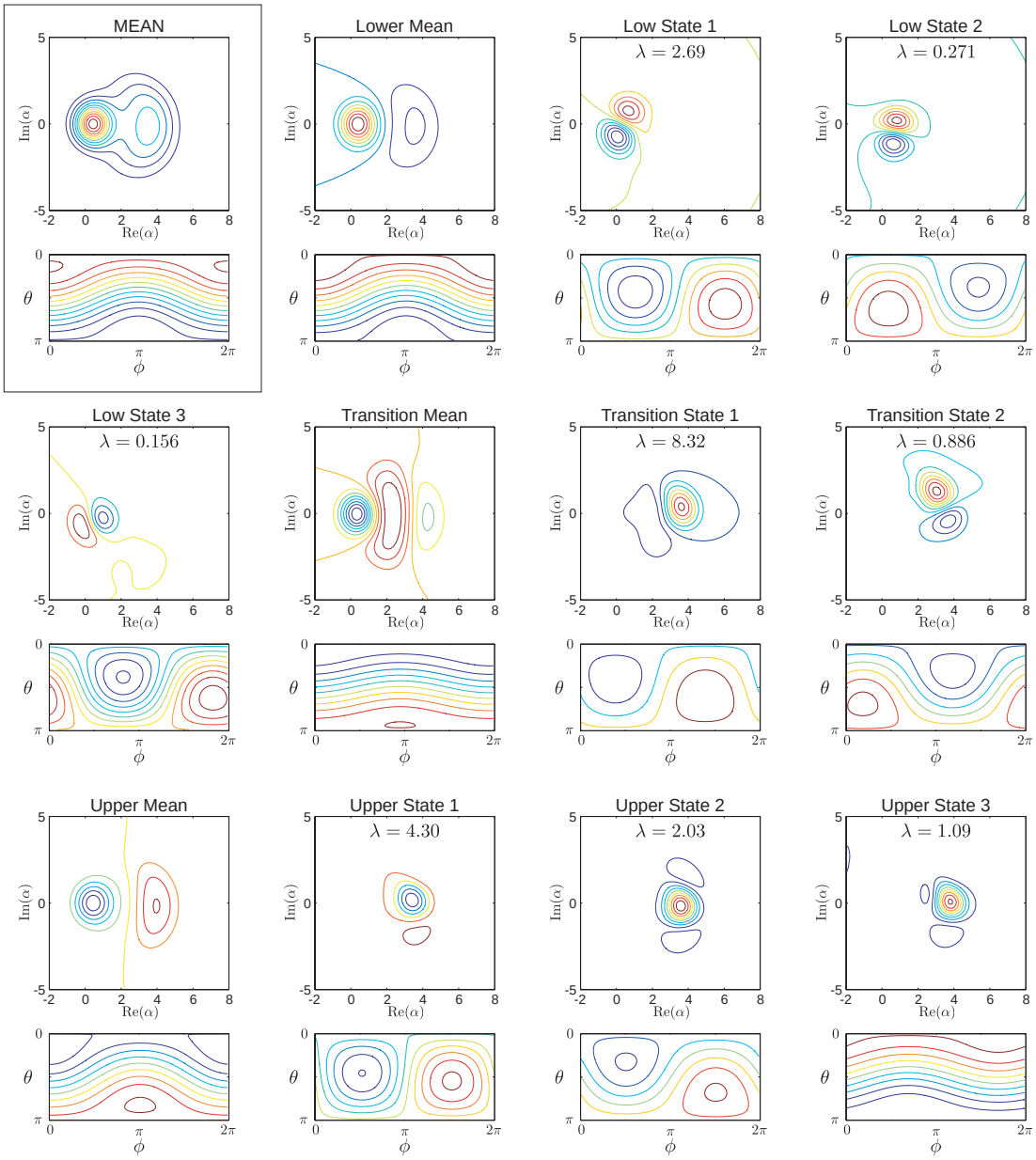

Figure 3.7: Contour plots of Q functions for states and basis vectors from "zoned" Proper Orthogonal Decomposition of absorptive bistability regime, with homodyne measurement of cavity field *amplitude* quadrature. The upper plot for each state is the Q function of the field state after tracing over the atom; the lower plot is the Q function of the atom after tracing over the field (produced using Generalized Coherent States [33]). Four states are generated separately from POD: the overall means state and the mean states in each of three zones. The leading 2 or 3 eigenstates from each zone are shown, along with the eigenvalue corresponding to each, showing the relative importance of each basis state/direction. The atomic Q functions are parametrized on a sphere spanned by $\theta \in [0, \pi]$ and $\phi \in [0, 2\pi]$.

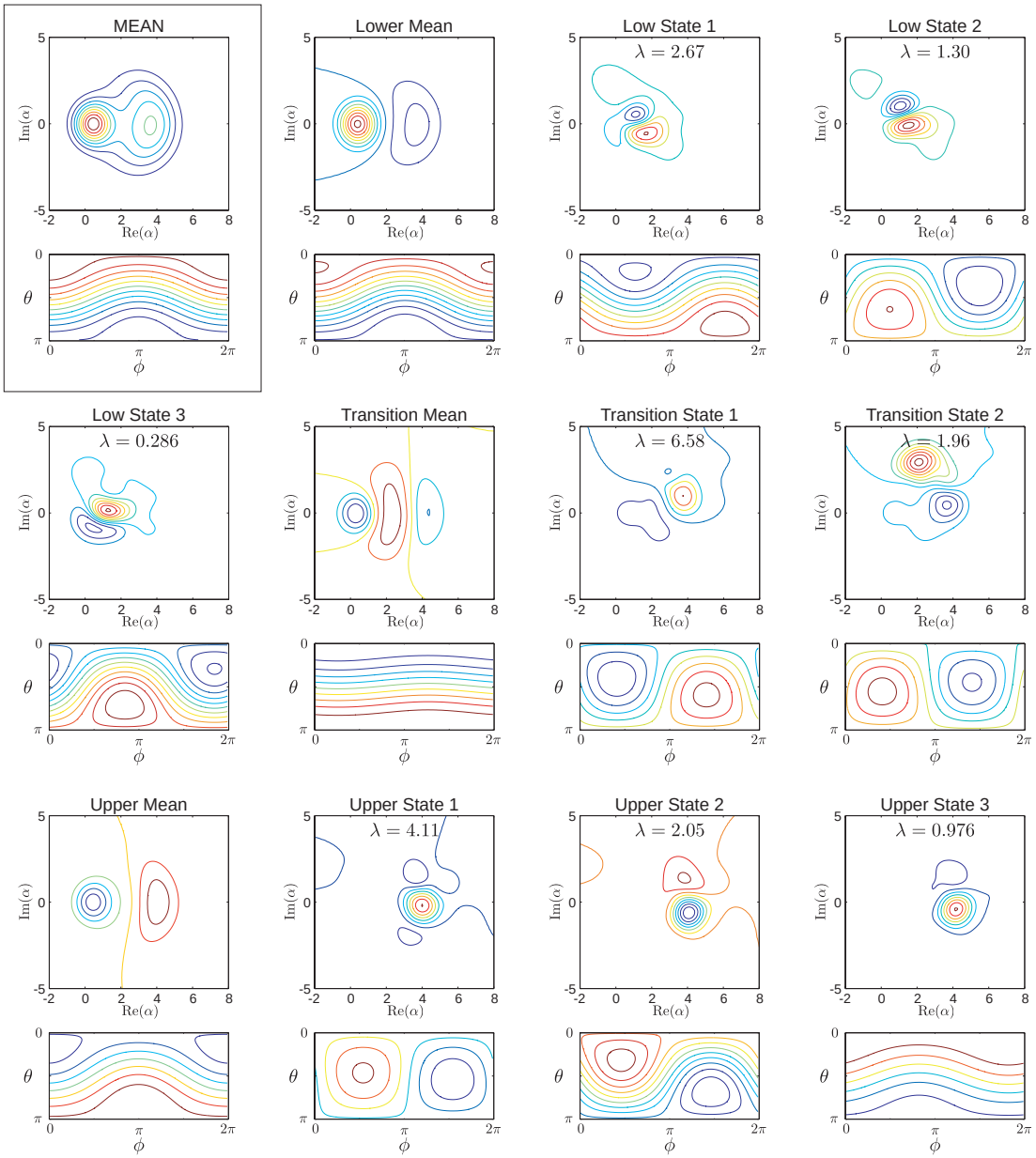

Figure 3.8: Contour plots of Q functions for states and basis vectors from "zoned" Proper Orthogonal Decomposition of absorptive bistability regime, with homodyne measurement of cavity field *phase* quadrature. The upper plot for each state is the Q function of the field state after tracing over the atom; the lower plot is the Q function of the atom after tracing over the field (produced using Generalized Coherent States [33]). Four states are generated separately from POD: the overall means state and the mean states in each of three zones. The leading 2 or 3 eigenstates from each zone are shown, along with the eigenvalue corresponding to each, showing the relative importance of each basis state/direction. The atomic Q functions are parametrized on a sphere spanned by $\theta \in [0, \pi]$ and $\phi \in [0, 2\pi]$.

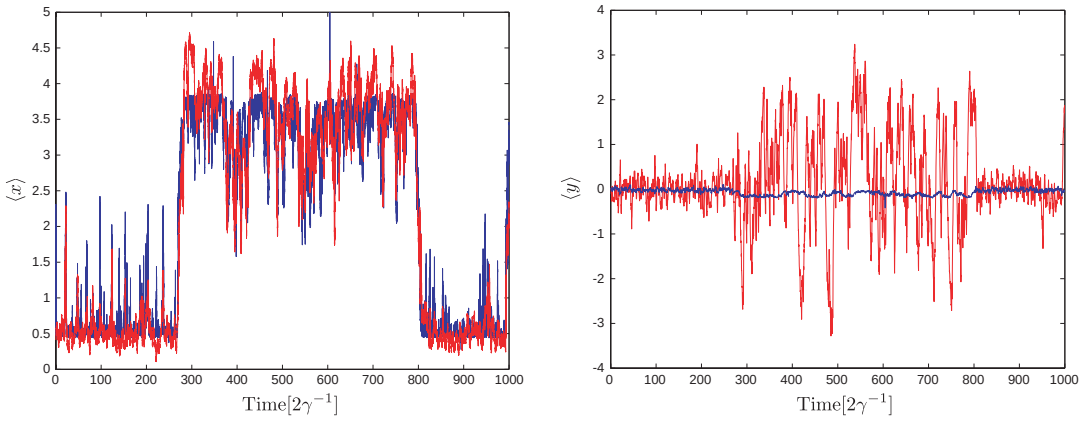

Figure 3.9: Comparison in the absorptive bistability regime of a "zoned" POD filter with exact quantum trajectory. The blue trace is the expected value of the amplitude quadrature for a POD filter with a 12-dimensional linear subspace; the red trace is from the quantum trajectory. The subspace is constructed from the mean states within each zone and the leading 3, 2, and 4 eigenstates from the lower, transition, and upper zones, respectively. Filter constructed and run on a system with a homodyne measurement on the amplitude quadrature.

is that we need to include more basis states, because we need the leading few from each zone. As an example, I chose to run the filter using a 12-dimensional subspace: the "lower mean" and the leading 3 eigenstates from the lower zone, "transition mean" and leading 2 eigenstates from the transition zone, and "upper mean" and 4 states from the upper zone. This means I am including 98.9% of the eigenvalue sum in the lower zone, 91.2% in the transition, and 98.3% in the upper zone, with 12 dimensions to consider (instead of 7 as in the basic POD filter above). As expected, this filter significantly outperforms the basic POD filter, helped immensely by its ability to successfully approximate both the lower and upper states. Figure 3.9 demonstrates the ability of the amplitude quadrature zoned filter to successfully capture the lower and upper states, as well as some of the dynamics within each. The large fluctuations within the upper state still prove to be too much for the "small amplitude" approximation built into the POD formulation.

The Probability of Error fidelity measure is somewhat better for the "zoned" POD than for the basic algorithm: at least the mean is positive (0.0134). The mean in the lower state is approximately 0.005, and it is somewhat better (0.027) in the upper state away from the few points where the filter becomes unphysical. The maximum Probability of Error for this data set was 0.09. The Bhattacharyya Coefficient similarly shows slight, but notable, improvement using the "zoned" algorithm relative to the basic POD process. The mean value of BC for this data set is 0.199 (compared to 0.185). The average in the lower state is about 0.17, and 0.22 in the upper state. Note that this reflects the markedly better performance for the zoned algorithm in the lower state and slightly worse performance in the upper state (perhaps due to the inclusion of only 4 eigenstates related to dynamics within that zone, compared with 6 in the simple POD algorithm).

If we discard the results of POD entirely, and use only the mean states for each zone, we end up with a reasonable filter, at least for amplitude quadrature behavior (it has no flexibility to capture the phase quadrature or atomic behavior). This 3-dimensional filter underperforms the 12-dimensional one, but might suffice for some applications. The mean Probability of Error is 0.0086 (with a mean of 0.0058 in the lower state, 0.0192 in the upper state, and a maximum of almost 0.08). The Bhattacharyya Coefficient is almost unchanged in this case for the lower state (where internal dynamics play a smaller role, so discarding them has a smaller effect), with a mean of 0.17. It performs less well in the upper state, as expected, with a mean of 0.215. The overall mean BC for this non-POD filter is 0.195.

The filter for homodyne measurement of the phase quadrature, using the same distribution of eigenstates as the amplitude quadrature, utterly fails as a reasonable filter. It behaves somewhat reasonably in the lower state, but fails in the upper state. To see why, look at the variation of the phase quadrature, $\langle y \rangle$, in Figure 3.9b, and compare it with the y-extent of the eigenstates in Figure 3.8. A filter based on the homodyne photocurrent from a phase quadrature measurement will attempt to match the observed value of the phase, but to do so given the eigenstates even from zoned POD requires unphysical states from combinations with large coefficients. In turn, these unphysical states do not do a good job of reproducing the other observables (like $\langle x \rangle$), and the fidelity of the filter to the actual dynamics is negligible (and the filter tends to be very unstable). This is not only a product of this "zoned" POD process: the same thing happens with basic, un-zoned POD, and with zoned basis states calculated using only the single overall mean (rather than the means for each zone).

3.5 Discussion

As we have seen in this chapter, Proper Orthogonal Decomposition is capable, when used with care and extended when necessary, of producing low-dimensional linear models which capture some of the dominant dynamics of quantum systems. Basic POD, applied to the phase bistable case, produced filters that are usually highly accurate at capturing the broad dynamics of the system, and might serve as reasonable filters for a control application. When extended into "zones," POD also works quite well for absorptive bistability, as long as the basis states used include close to the full range for the variable being measured (the amplitude quadrature for our example).

POD is not a universal tool, however, and its limitations in both the phase and absorptive bistability regimes illustrate broader issues that would arise should the tool be extended to other systems. The first of these is the algorithm's tendency to deliver spaces which include only the type of dynamics in which the system spends the largest fraction of the time. In the phase bistable case, the particular trajectory used as an example in this thesis spends slightly more time in one

state than the other. As a result, the basis set returned by POD favors some dynamics within this slightly-favored state over dimensions that inform us about state transitions; this may not match the order in which the experimentalist would emphasize these two behaviors.

This sensitivity to asymmetry is also at play in the absorptive bistability example, and is exacerbated by shape asymmetry between the upper and lower states. The definition of distance in the density-matrix space, which is the most obvious choice for that metric, also contributes significantly to this behavior. Even drastic interventions in this definition of distance, however, were unable to qualitatively change the POD algorithm's behavior (and resulting failing filter) to match the physical system's behavior.

At the root of concerns about asymmetry and distance is the fundamental limitation of Proper Orthogonal Decomposition: it only captures directions away from a mean state, defines a linear space, and fundamentally relates only to small perturbations away from the mean. Large dynamics away from the mean and nonlinear underlying structures of the dynamics (such as multiple stable states) all challenge POD in precisely this weak spot. Unfortunately, it is often precisely this behavior which we wish to capture or control.